Group-VII point defects in ZnSe

L. S. dos Santos, W. G. Schmidt, and E. Rauls
Lehrstuhl für Theoretische Physik, Universität Paderborn, D-33095 Paderborn, Germany
(Received 2 May 2011; revised manuscript received 26 July 2011; published 2 September 2011)

Zinc selenide (ZnSe) is a promising material for applications in quantum computing. Only recently, it was shown that fluorine-doped ZnSe may serve as a source for indistinguishable photons. We have studied both chlorine and fluorine point defects in ZnSe by means of first-principles density functional theory calculations. The incorporation of F or Cl, either isolated, pairwise, or in combination with Zn or Se vacancies, has been investigated thoroughly for a large variety of possible charge states. For the most important structures, computationally more demanding calculations, with a hybrid functional rather than the generalized gradient approximation for the treatment of electron exchange and correlation, have been carried out. This was found to have little effect on the energetical order of the defect, but considerably changes the absolute formation energies of the defects.

DOI: 10.1103/PhysRevB.84.115201 PACS number(s): 61.50.Ah, 61.72.Bb, 61.72.J−

I. INTRODUCTION

Zinc selenide (ZnSe) is an extensively studied semiconductor of the II-VI groups. Point defects for *p*- or *n*-type doping of ZnSe have been intensively studied, both theoretically and experimentally. Many studies have aimed at gaining a deeper understanding of the difficulties in *p*-type doping. Early density functional theory calculations were made by Laks *et al.*[1] for this purpose. García and Northrup's study,[2] based on local density approximation calculations, indicated that dopant-vacancy complexes (for example, $As_{Se}V_{Se}$) could play an important role in the self-compensation mechanism that limits doping efficiency.

Pöykkö *et al.* published theoretical studies about chlorine[3] (an *n*-type donor) and nitrogen[4] (a *p*-type acceptor) in ZnSe. These studies also highlighted the importance of impurity-defect complexes in doping compensation, in particular the substitutional chlorine-zinc vacancy ($Cl_{Se}V_{Zn}$) and the substitutional nitrogen-zinc vacancy ($N_{Se}V_{Se}$) complexes, which are pointed out as strong candidates for the compensating center in the respective cases.

Saarinen *et al.*[5] have used positron annihilation spectroscopy to directly identify vacancies in N-doped and Cl-doped ZnSe, suggesting that vacancies are involved in the compensation mechanism. A later study by Gebauer *et al.*[6] obtained similar conclusions, attributing the compensation mechanism in *n*-doped ZnSe to V_{Zn}-donor complexes.

Nowadays, ZnSe is experiencing a renaissance as a material with properties most appropriate for application in quantum computing. Recently, Yamamoto *et al.*[7] have shown that independent ZnSe quantum wells doped with fluorine can emit indistinguishable photons, which can be used to encode and transport information. With its potential application in quantum computing, fluorine turns out to have even better properties as an *n*-type dopant in ZnSe than chlorine due to the isotopic purity, which makes all emitted electrons indistinguishable in the case of fluorine. However, very little is known about the microscopic structure of F-related point defects in ZnSe.

In order to contribute to a better understanding of this mechanism, we performed density functional calculations on F-related point defects in ZnSe. The results are compared to calculations on Cl-related point defects, for which previous theoretical data are available. In addition to the isolated flourine, we also considered native defects (such as vacancies), defect pairs (Cl-Cl and F-F), and mixed impurity-native complexes such as $Cl_{Se}V_{Zn}$. The complete set of considered defects is shown in Tables I to IV. Generalized gradient approximation (GGA)-based calculations (cf. next section) were performed for all defects in all charge states ranging from −2 to +3.

In addition, selected defects and charge states, especially those with low formation energies in the GGA, were investigated with the help of hybrid functionals [Heyd, Scuseria, and Ernzerhof (HSE)]. Since in HSE the experimental band gap of ZnSe is reproduced, the results of these calculations are expected to be closer to the experimental results, however, at the expense of substantially increased computational costs.

II. CALCULATION METHODS

The density functional theory (DFT) calculations were performed in the projector-augmented-wave (PAW)[8] formalism with the PW91 GGA description[9] for the exchange-correlation energies, as implemented in the VIENNA AB INITIO SIMULATION PACKAGE (VASP). A cubic supercell with 64 atoms was used, corresponding to 2 × 2 × 2 cubic unit cells. An energy cutoff of 400 eV was used. The special **k** point $(\frac{1}{4},\frac{1}{4},\frac{1}{4})$ was used for the Brillouin-zone sampling. Each defect was relaxed to its lowest energy configuration starting from slightly randomized atomic positions to allow for possible symmetry breaking. The supercell shape was kept fixed during relaxation. For various defects, convergence with supercell size has been checked with a 216-atom cell, showing no significant changes. The same holds for the **k**-point sampling, which was tested with (2 × 2 × 2) **k**-point sets. For consistency reasons (i.e., compared to the literature and for our additional hybrid calculations), we only present the results for the 64-atom cell.

For the hybrid functional calculations (contained in Table V), we used a slightly modified version of the HSE06 functional.[10] The modification consists of increasing the fraction of exact exchange to 32%, as compared to 25% in standard HSE06. It was found that this setting results in a much better prediction of the band gap than standard HSE06, which still significantly underestimates the band gap in ZnSe.

TABLE I. Native defects. The second column gives the point group of the defect and the number of orientations in which it can appear in the ZnSe lattice (which has T_d symmetry). The next two columns give our calculated formation energy under standard conditions (see text for details), followed by García and Northrup's values for comparison.[2] All values are given in electron volts (eV).

Defect	Symmetry	Ω^0	Ω^0 [2]
V_{Se}^{0}	C_{1h} (12)	2.05	2.70
V_{Se}^{+1}	C_3 (8)	1.30	1.64
V_{Se}^{+2}	C_{3v} (4)	− 0.79	− 0.49
V_{Se}^{+3}	C_{3v} (4)	− 0.77	
V_{Se}^{-1}	C_1 (24)	3.91	
V_{Se}^{-2}	C_1 (24)	5.13	
$V_{Se}V_{Zn}^{0}$	C_{3v} (4)	2.08	
$V_{Se}V_{Zn}^{+1}$	C_{3v} (4)	1.98	
$V_{Se}V_{Zn}^{+2}$	C_{3v} (4)	1.96	
$V_{Se}V_{Zn}^{+3}$	C_{3v} (4)	2.00	
$V_{Se}V_{Zn}^{-1}$	C_{1h} (12)	4.11	
$V_{Se}V_{Zn}^{-2}$	C_{3v} (4)	4.81	
V_{Zn}^{0}	C_{3v} (4)	3.33	
V_{Zn}^{+1}	C_{3v} (4)	3.22	
V_{Zn}^{+2}	C_{3v} (4)	3.14	
V_{Zn}^{+3}	C_{3v} (4)	3.31	
V_{Zn}^{-1}	C_{3v} (4)	3.49	
V_{Zn}^{-2}	T_d (1)	3.72	

By starting the calculations from the atomic structure obtained from optimization within the standard DFT calculation, we performed a full optimization within the HSE calculation. An energy cutoff of 400 eV was used once again, but this time with a regular, Γ-centered, $2 \times 2 \times 2$ **k**-point grid. In most cases, convergence was reached after only a few further relaxation steps, resulting in energy differences below 0.1 eV compared to the DFT-relaxed geometries.

III. DEFECT FORMATION ENERGIES AND CONCENTRATIONS

The concentration of a point defect in a semiconductor crystal is essentially determined by the defect's formation energy,[11]

$$c = n_{\text{sites}}\, n_{\text{configs}}\, e^{-\Omega/kT}, \tag{1}$$

where n_{sites} is the number of lattice sites where the defect can be incorporated and n_{configs} is the number of symmetry configurations in which the defect can be incorporated (this is for defects with the same symmetry as the underlying crystal lattice, and correspondingly larger than the one when symmetry breaking occurs). The defect formation energy (represented by Ω) can be obtained from *ab initio* thermodynamics.[12] For neutral defects, we have

$$\Omega = E_{\text{def}} - E_{\text{bulk}} - \sum_i n_i\, \mu_i, \tag{2}$$

where E_{def} is the energy of the defect supercell, E_{bulk} is the energy of the ideal crystal cell (bulk), and n_i is the number of atoms of species i that is added to (positive) or removed from (negative) the ideal crystal to create the defect, with the corresponding chemical potential μ_i.

TABLE II. Chlorine-containing defects. The first three columns mean the same as in Table I. In the fourth column, Ω is the formation energy obtained by setting $\mu_{\text{Cl}} = \frac{1}{2}E_{\text{DFT}}(\text{Cl}_2)$, which can be directly compared with the reference values from Nieminen *et al.*[3] in the last column. All values are given in electron volts (eV).

Defect	Symmetry	Ω^0	Ω	Ω [3]
Cl_{Se}^{0}	C_{3v} (4)	− 2.14	− 0.38	
Cl_{Se}^{+1}	C_{3v} (4)	− 4.48	− 2.72	− 1.13
Cl_{Se}^{+2}	C_{3v} (4)	− 4.61	− 2.85	
Cl_{Se}^{+3}	C_{3v} (4)	− 4.70	− 2.94	
Cl_{Se}^{-1}	C_{3v} (4)	0.22	1.98	
Cl_{Se}^{-2}	C_{3v} (4)	2.97	4.73	
Cl_{Zn}^{0}	C_{1h} (12)	1.54	3.30	
Cl_{Zn}^{+1}	C_{1h} (12)	1.20	2.96	5.38
Cl_{Zn}^{+2}	C_{1h} (12)	0.83	2.59	
Cl_{Zn}^{+3}	C_1 (24)	0.57	2.33	
Cl_{Zn}^{-1}	C_{1h} (12)	1.88	3.64	
Cl_{Zn}^{-2}	C_{1h} (12)	4.02	5.78	5.46
$Cl_i(T_{Zn})^{0}$	C_{1h} (12)	0.64	2.40	
$Cl_i(T_{Zn})^{+1}$	C_{1h} (12)	0.28	2.04	3.71
$Cl_i(T_{Zn})^{+2}$	C_{1h} (12)	− 0.03	1.73	
$Cl_i(T_{Zn})^{+3}$	C_{1h} (12)	− 0.30	1.46	
$Cl_i(T_{Zn})^{-1}$	C_{1h} (12)	1.06	2.82	3.75
$Cl_i(T_{Zn})^{-2}$	C_{1h} (12)	3.62	5.38	
$Cl_i(T_{Se})^{0}$	C_1 (24)	0.45	2.21	
$Cl_i(T_{Se})^{+1}$	C_1 (24)	− 1.14	0.62	2.01
$Cl_i(T_{Se})^{+2}$	C_1 (24)	− 1.41	0.35	
$Cl_i(T_{Se})^{+3}$	C_1 (24)	− 1.66	0.10	
$Cl_i(T_{Se})^{-1}$	C_{1h} (12)	1.06	2.82	4.92
$Cl_i(T_{Se})^{-2}$	C_{1h} (12)	3.62	5.38	
$Cl_{Se}V_{Zn}^{0}$	C_{1h} (12)	− 1.47	0.29	
$Cl_{Se}V_{Zn}^{+1}$	C_{1h} (12)	− 1.61	0.15	
$Cl_{Se}V_{Zn}^{+2}$	C_{1h} (12)	− 1.69	0.07	
$Cl_{Se}V_{Zn}^{+3}$	C_1 (24)	− 1.72	0.04	
$Cl_{Se}V_{Zn}^{-1}$	C_1 (24)	− 1.25	0.51	2.11
$Cl_{Se}V_{Zn}^{-2}$	C_1 (24)	1.03	2.79	
$Cl_{Se}V_{Se}^{0}$	C_1 (24)	− 0.83	0.93	
$Cl_{Se}V_{Se}^{+1}$	C_{1h} (12)	− 2.73	− 0.97	1.11
$Cl_{Se}V_{Se}^{+2}$	C_{1h} (12)	− 3.19	− 1.43	
$Cl_{Se}V_{Se}^{+3}$	C_{1h} (12)	− 5.03	− 3.27	− 0.82
$Cl_{Se}V_{Se}^{-1}$	C_{1h} (12)	0.31	2.07	3.92
$Cl_{Se}V_{Se}^{-2}$	C_1 (24)	2.52	4.28	

For a single-component crystal, the chemical potential μ is uniquely determined by the total energy. In the case of a two-component crystal such as ZnSe, where we have

$$\Omega = E_{\text{def}} - E_{\text{bulk}} - n_{\text{Zn}}\,\mu_{\text{Zn}} - n_{\text{Se}}\,\mu_{\text{Se}} - n_{\text{imp}}\,\mu_{\text{imp}}, \tag{3}$$

(n_{imp} and μ_{imp} refer to an impurity atom, which in this study is either Cl or F), the chemical potentials for Zn and Se are not uniquely determined by the total energy, but depend on the crystal growth conditions.

Some boundaries can be established for these chemical potentials.[2] The energy condition gives us $\mu_{\text{Zn}} + \mu_{\text{Se}} = E_{\text{ZnSe}}$, where E_{ZnSe} is the total energy of a pair of atoms in the crystal

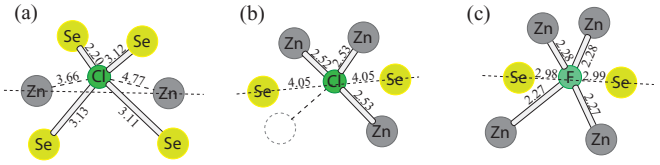

FIG. 1. (Color online) Equilibrium geometries after structural relaxation. (a) Cl_{Zn}^{+3} [an equivalent geometry results from relaxation of $Cl_i(T_{Se})V_{Zn}$]. (b) $Cl_{Se}V_{Zn}^{-1}$ (equivalent geometry results from $Cl_{Zn}V_{Se}$). (c) $F_i(T_{Zn})^{-1}$ [equivalent geometry results from $F_i(T_{Se})$ for negative charge states].

(one Zn atom plus one Se atom). We must also have $\mu_{Se} \leqslant \mu_{Se}(\text{bulk})$, otherwise bulk Se would be more stable than the ZnSe crystal and precipitation would occur, forming a bulk Se phase. The same can be said for Zn: $\mu_{Zn} \leqslant \mu_{Zn}(\text{bulk})$.

These three restrictions limit the allowed range of variation of μ_{Zn} and μ_{Se}. This variation is commonly described by a parameter λ which varies between zero and one, as done, for example, by García and Northrup:[2]

$$\mu_{Zn} = \mu_{Zn}(\text{bulk}) + \lambda\,\Delta H, \tag{4}$$

$$\mu_{Se} = \mu_{Se}(\text{bulk}) + (1-\lambda)\,\Delta H, \tag{5}$$

where ΔH is the formation energy of ZnSe, defined as $\Delta H = E_{ZnSe} - \mu_{Zn}(\text{bulk}) - \mu_{Se}(\text{bulk})$. Our GGA calculations result in $\Delta H = -1.45$ eV. Note that, in contrast to Ref. 2, we adopt a negative sign for ΔH, keeping with the convention that exothermic formation energies are negative. In Eqs. (4) and (5), $\lambda = 0$ corresponds to Zn-rich conditions, in which μ_{Zn} takes the maximum allowed value, whereas $\lambda = 1$ corresponds to Se-rich conditions.

Substituting Eqs. (4) and (5) in Eq. (3) results in

$$\Omega(\lambda, \mu_{\text{imp}}, E_F) = \Omega^0 - \lambda\,\Delta H(n_{Zn} - n_{Se}) + n_{\text{imp}}\,\mu_{\text{imp}} + q\,(E_F + E_{VBM} + \Delta V), \tag{6}$$

where we have added a term related to the defect charge q to account for charged defects. E_F denotes the Fermi level measured relative to the valence-band maximum, E_{VBM} is the energy of an electron at the *valence-band maximum* of the ideal crystal, and ΔV is a band-alignment term,[11] determined by calculating the average electrostatic potential in the defect cell along the z direction and comparing it to the corresponding potential for the ideal cell. The band-alignment differences occurring in our calculations are of the order of 0.1–0.3 eV for most defect cells, which is probably smaller than other sources of error in our calculations.

In good approximation, E_{VBM} is determined by the resulting energy difference when a very small fraction of an electron (say, 0,001 e) is removed from a neutral ZnSe cell. We performed two DFT calculations, one for the neutral cell and one for the cell with charge +0.001, and determine E_{VBM} as follows:[13]

$$E_{VBM} = \frac{E^0_{\text{bulk}} - E^{+0.001}_{\text{bulk}}}{0.001}. \tag{7}$$

Our GGA calculations for ZnSe give $E_{VBM} = 1.21$ eV.

The quantity Ω^0 in Eq. (6) refers to the defect formation energy under the following standard conditions: $\lambda = 0$ (Zn-rich growth), $E_F = 0$ (Fermi energy at valence-band maximum), and $\mu_{\text{imp}} = 0$. It is given by the following expression:

$$\Omega^0 = E_{\text{tot}}(\text{defect}) + \mu_{Zn}(\text{bulk})(n_{Se} - n_{Zn}) - E_{ZnSe}\,n_{Se}, \tag{8}$$

where $E_{\text{tot}}(\text{defect})$ is the GGA total energy. Our calculations on bulk Zn, Se, and ZnSe give $\mu_{Zn}(\text{bulk}) = -1.1268$ eV and $E_{ZnSe} = -6.0810$ eV, in good agreement with experimental values.

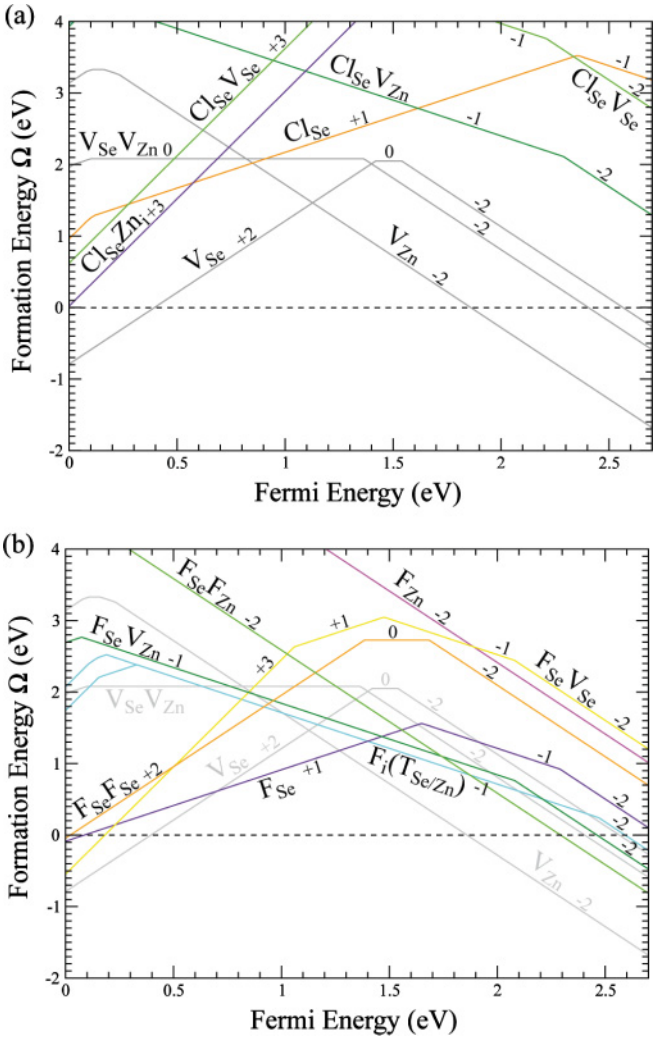

FIG. 2. (Color online) Formation energies of defects at $\lambda = 0$ (Zn-rich condition) with $\mu_{Cl/F}$ fixed. (a) Chlorine defects (this graph uses the same conditions as Ref. 3). (b) Fluorine defects.

Equations (6) and (8) form our model for the calculation of defect formation energies. This model will be used in the next section to determine defect formation energies and concentrations. The parameters λ and E_F are set to fixed values to reproduce the conditions that we wish to simulate. The parameter μ_{imp} requires special treatment, as ZnSe crystals are typically grown by molecular-beam epitaxy (MBE), a nonequilibrium process, and therefore the chemical potential μ_{imp} of an impurity in the crystal is in principle unrelated to the chemical potentials of precursor gases in the MBE process. Instead of setting a fixed value for μ_{imp}, we set a value for the impurity concentration ($c_{\text{imp}} = 5 \times 10^{17}/\text{cm}^3$), which is a directly measurable parameter, and solve numerically for the

TABLE III. Chlorine-containing defects (part 2). The meaning of the columns is the same as in Table II. All values are given in electron volts (eV). Defect structures marked with a dot in front are not stable in the given configuration, but spontaneously transform to another defect, which already appeared in Table II (see text for details).

Defect	Symmetry	Ω^0	Ω	Ω [3]
$\cdot Cl_i(T_{Se})V_{Zn}{}^0$	C_{1h} (12)	1.54	3.30	
$\cdot Cl_i(T_{Se})V_{Zn}{}^{+1}$	C_{1h} (12)	1.20	2.96	3.32
$\cdot Cl_i(T_{Se})V_{Zn}{}^{+2}$	C_{1h} (12)	0.83	2.59	
$\cdot Cl_i(T_{Se})V_{Zn}{}^{+3}$	C_1 (24)	0.57	2.33	2.03
$\cdot Cl_i(T_{Se})V_{Zn}{}^{-1}$	C_1 (24)	1.88	3.64	5.18
$\cdot Cl_i(T_{Se})V_{Zn}{}^{-2}$	C_1 (24)	3.97	5.73	
$\cdot Cl_{Zn}V_{Se}{}^0$	C_{3v} (4)	− 1.47	0.29	
$Cl_{Zn}V_{Se}{}^{+1}$	C_{1h} (12)	− 0.33	1.43	4.30
$Cl_{Zn}V_{Se}{}^{+2}$	C_1 (24)	− 0.54	1.22	
$Cl_{Zn}V_{Se}{}^{+3}$	C_{1h} (12)	− 0.75	1.01	
$\cdot Cl_{Zn}V_{Se}{}^{-1}$	C_{3v} (4)	− 1.25	0.51	
$\cdot Cl_{Zn}V_{Se}{}^{-2}$	C_{3v} (4)	1.03	2.79	
$Cl_{Se}Zn_i{}^0$	C_1 (24)	− 0.14	1.62	
$Cl_{Se}Zn_i{}^{+1}$	C_{1h} (12)	− 2.49	− 0.73	0.73
$Cl_{Se}Zn_i{}^{+2}$	C_{1h} (12)	− 3.61	− 1.85	
$Cl_{Se}Zn_i{}^{+3}$	C_{1h} (12)	− 5.64	− 3.88	
$Cl_{Se}Zn_i{}^{-1}$	C_1 (24)	1.79	3.55	
$Cl_{Se}Zn_i{}^{-2}$	C_1 (24)	4.34	6.10	
$Cl_{Se}Cl_{Se}{}^0$	C_1 (24)	− 4.35	− 0.83	
$Cl_{Se}Cl_{Se}{}^{+1}$	C_1 (24)	− 6.64	− 3.12	
$Cl_{Se}Cl_{Se}{}^{+2}$	C_1 (24)	− 8.92	− 5.40	
$Cl_{Se}Cl_{Se}{}^{+3}$	C_1 (24)	− 8.99	− 5.47	
$Cl_{Se}Cl_{Se}{}^{-1}$	C_1 (24)	− 2.44	1.08	
$Cl_{Se}Cl_{Se}{}^{-2}$	C_1 (24)	− 0.20	3.32	
$Cl_{Se}Cl_{Zn}{}^0$	C_1 (24)	− 3.64	− 0.12	
$Cl_{Se}Cl_{Zn}{}^{+1}$	C_1 (24)	− 3.92	− 0.40	
$Cl_{Se}Cl_{Zn}{}^{+2}$	C_1 (24)	− 4.21	− 0.69	
$Cl_{Se}Cl_{Zn}{}^{+3}$	C_1 (24)	− 4.32	− 0.80	
$Cl_{Se}Cl_{Zn}{}^{-1}$	C_1 (24)	− 1.82	1.70	
$Cl_{Se}Cl_{Zn}{}^{-2}$	C_1 (24)	− 1.19	2.33	

value of μ_{imp} that will result in the desired concentration. The total impurity concentration is given by

$$c_{\text{imp}} = \sum_i n_i\, c_i\,, \tag{9}$$

where the sum is over all defects, n_i is the number of impurity atoms in a supercell of defect i, and c_i is the concentration of defect i, given by Eq. (1). Given a constant value for c_{imp}, Eq. (9) can be solved numerically for μ_{imp}, resulting in an effective chemical potential that is valid for specific values of λ and E_F.

The above procedure is only valid if all relevant defects are included in the sum. The relevant defects are all defects with relatively low formation energy. Since the concentration of any given defect falls off exponentially with the increase in Ω, by a factor of $\exp(-\Omega/kT)$, an increase of only 0.7 eV in Ω results in a lowered defect concentration by a factor greater than 10^{-4}. Therefore, the omission of any defect with a relatively high formation energy (i.e., at least 0.7 eV higher than the formation energy of the most stable defect) from Eq. (9) will have a negligible effect on the result.

TABLE IV. Fluorine-containing defects. The meaning of the columns is the same as in Table I. All values are given in electron volts (eV).

Defect	Symmetry	Ω^0	Defect	Symmetry	Ω^0
$F_{Se}{}^0$	C_1 (24)	-3.38	$F_{Se}V_{Se}{}^0$	C_1 (24)	-2.02
$F_{Se}{}^{+1}$	C_1 (24)	-5.58	$F_{Se}V_{Se}{}^{+1}$	C_1 (24)	-3.92
$F_{Se}{}^{+2}$	C_1 (24)	-5.60	$F_{Se}V_{Se}{}^{+2}$	C_1 (24)	-4.22
$F_{Se}{}^{+3}$	C_1 (24)	-5.59	$F_{Se}V_{Se}{}^{+3}$	C_1 (24)	-6.04
$F_{Se}{}^{-1}$	C_1 (24)	-2.28	$F_{Se}V_{Se}{}^{-1}$	C_1 (24)	-0.97
$F_{Se}{}^{-2}$	C_1 (24)	0.01	$F_{Se}V_{Se}{}^{-2}$	C_1 (24)	1.11
$F_{Zn}{}^0$	C_1 (24)	-0.30	$F_{Se}V_{Zn}{}^0$	C_{1h} (12)	-2.76
$F_{Zn}{}^{+1}$	C_1 (24)	-0.45	$F_{Se}V_{Zn}{}^{+1}$	C_{1h} (12)	-2.80
$F_{Zn}{}^{+2}$	C_{1h} (12)	-0.53	$F_{Se}V_{Zn}{}^{+2}$	C_{1h} (12)	-2.70
$F_{Zn}{}^{+3}$	C_{1h} (12)	-0.54	$F_{Se}V_{Zn}{}^{+3}$	C_{3v} (4)	-2.64
$F_{Zn}{}^{-1}$	C_1 (24)	-0.04	$F_{Se}V_{Zn}{}^{-1}$	C_1 (24)	-2.65
$F_{Zn}{}^{-2}$	C_{3v} (4)	0.92	$F_{Se}V_{Zn}{}^{-2}$	C_{3v} (4)	-0.57
$F_i(T_{Se})^0$	C_{1h} (12)	-2.99	$F_{Se}F_{Se}{}^0$	C_1 (24)	-8.26
$F_i(T_{Se})^{+1}$	C_1 (24)	-3.44	$F_{Se}F_{Se}{}^{+1}$	C_1 (24)	-9.02
$F_i(T_{Se})^{+2}$	C_1 (24)	-3.61	$F_{Se}F_{Se}{}^{+2}$	C_1 (24)	-11.03
$F_i(T_{Se})^{+3}$	C_1 (24)	-3.75	$F_{Se}F_{Se}{}^{+3}$	C_1 (24)	-10.89
$F_i(T_{Se})^{-1}$	C_{1h} (12)	-2.78	$F_{Se}F_{Se}{}^{-1}$	C_1 (24)	-6.30
$F_i(T_{Se})^{-2}$	C_{3v} (4)	-0.31	$F_{Se}F_{Se}{}^{-2}$	C_1 (24)	-4.89
$F_i(T_{Zn})^0$	C_1 (24)	-2.98	$F_{Se}F_{Zn}{}^0$	C_1 (24)	-6.50
$F_i(T_{Zn})^{+1}$	C_{1h} (12)	-3.16	$F_{Se}F_{Zn}{}^{+1}$	C_1 (24)	-6.65
$F_i(T_{Zn})^{+2}$	C_{1h} (12)	-3.31	$F_{Se}F_{Zn}{}^{+2}$	C_1 (24)	-6.66
$F_i(T_{Zn})^{+3}$	C_{1h} (12)	-3.42	$F_{Se}F_{Zn}{}^{+3}$	C_{1h} (12)	-6.57
$F_i(T_{Zn})^{-1}$	C_{1h} (12)	-2.78	$F_{Se}F_{Zn}{}^{-1}$	C_1 (24)	-6.53
$F_i(T_{Zn})^{-2}$	C_1 (24)	-0.31	$F_{Se}F_{Zn}{}^{-2}$	C_1 (24)	-6.40

IV. RESULTS AND DISCUSSION

Tables I to IV show our DFT formation energies and defect symmetries. The energies given are Ω_0, that is, they have been calculated at $\lambda = 0$, $E_F = 0$, and $\mu_{Cl/F} = 0$. The formation energy under arbitrary conditions can be easily obtained with (6). We have compared some of our results for native defects in Table I with those by García and Northrup[2] (available only for a few defects), with generally good agreement. For the chlorine defects in Tables II and III, we have compared the formation energies with the data of Nieminen *et al.*[3] They have given their formation energies with the chemical potential of chlorine taken from the DFT total energy of a chlorine molecule, $\mu_{Cl} = \frac{1}{2}E_{DFT}(Cl_2)$, instead of $\mu_{Cl} = 0$. Therefore, we provide the same data in Tables II and III to allow for a direct comparison. In this case, we observe deviations that are typically larger than 1 eV. However, the qualitative picture, i.e., which defects are the most stable, remains unchanged.

Another thing to notice in the data of Tables I to IV is that some defects have nearly identical energies. This happens in the case of $Cl_i(T_{Se})V_{Zn}$ and Cl_{Zn}, which have practically identical DFT energies and formation energies, for the respective charge states. As these two defects have the same number of atoms (one Cl atom added and one Zn atom removed, respectively), during structural relaxation they relax to the same equilibrium configuration, in which the Cl atom is close to the position where the Zn atom would be, but in an asymmetrical position, as depicted in Fig. 1(a).

TABLE V. Comparison of the formation energies between GGA and hybrid functional (HSE) calculations. As before, Ω^0 is the defect formation energy taken at $\lambda = 0$, $E_F = 0$, and $\mu_{Cl/F} = 0$. All values are given in electron volts (eV).

Defect	Ω^0 GGA	Ω^0 HSE
V_{Se}^{+2}	−0.79	−2.05
$V_{Se}V_{Zn}^{-2}$	4.81	6.69
V_{Zn}^{-2}	3.72	5.43
Cl_{Se}^{+1}	−4.48	−8.70
Cl_{Se}^{+2}	−4.61	−8.73
Cl_{Se}^{+3}	−4.70	−8.71
$Cl_{Se}V_{Zn}^{-1}$	−1.25	−3.93
$Cl_{Se}Cl_{Se}^{+2}$	−8.92	−16.16
$Cl_{Se}Cl_{Se}^{+3}$	−8.99	−16.21
F_{Se}^{+1}	−5.58	−10.75
F_{Se}^{+2}	−5.60	−10.70
F_{Se}^{+3}	−5.59	−10.59
$F_{Se}V_{Se}^{+3}$	−6.04	−12.55
$F_{Se}F_{Se}^{+2}$	−11.03	−21.40
$F_{Se}F_{Se}^{+3}$	−10.89	−21.27
$F_{Se}F_{Zn}^{-2}$	−6.40	−13.82

The same thing happens to $Cl_{Zn}V_{Se}$ and $Cl_{Se}V_{Zn}$, which also end up with identical energies. In this case, the Cl atoms migrate during relaxation from the Zn position to the Se position, that is, $Cl_{Zn}V_{Se}$ spontaneously converts to $Cl_{Se}V_{Zn}$. In the case of the defect pairs $Cl_i(T_{Se})/Cl_i(T_{Zn})$ and $F_i(T_{Se})$, $F_i(T_{Zn})$, the same is observed for negative charge states, where the T_{Zn} position appears to be preferred.

The equilibrium configuration of most defects is highly asymmetrical. Cl_{Se} shows only C_{3v} symmetry (deformation in the [111] direction), and the previously mentioned Cl_{Zn} (Fig. 1) is only C_{1h}/C_1. The symmetries shown in the tables have been determined with a tolerance of approximately 0.11 Å for atomic positions.

The numbers given in parentheses in the symmetry column of Tables I to IV refer to the number of different orientations in which a defect can appear in the crystal lattice of ZnSe, which has T_d symmetry. This number appears as the term $n_{configs}$ in Eq. (1), which defines defect concentrations.

Figure 2(a) shows the formation energies Ω for defects as a function of the Fermi energy. These formation energies have been calculated using fixed chemical potentials, $\mu_{Cl} = \frac{1}{2}E_{DFT}(Cl_2)$. They are directly comparable to those of Pöykkö *et al.*[3] In general, our formation energies are about 2 eV higher than those of the literature reference. Despite an intensive search for possible explanations, including numerous test calculations, among them some with 216-atom cells, we failed to determine the cause of this discrepancy.

Nevertheless, the qualitative picture is similar. In general, among the native defects, the doubly negative Zn vacancy is found to be most abundant in MBE-grown samples.[14] This is confirmed by our calculations. By adding impurities, both our work and Ref. 3 indicate Cl_{Se}^{+1} as the most stable chlorine defect in a range of E_F from 0.6 eV to about 1.6 eV. When E_F is higher than 1.6 eV, both works indicate $Cl_{Se}V_{Zn}$ as the most stable defect. For low values of E_F (below about 0.6 eV), there is a difference. Our results indicate that $Cl_{Se}Zn_i^{+3}$ and $Cl_{Se}V_{Se}^{+3}$

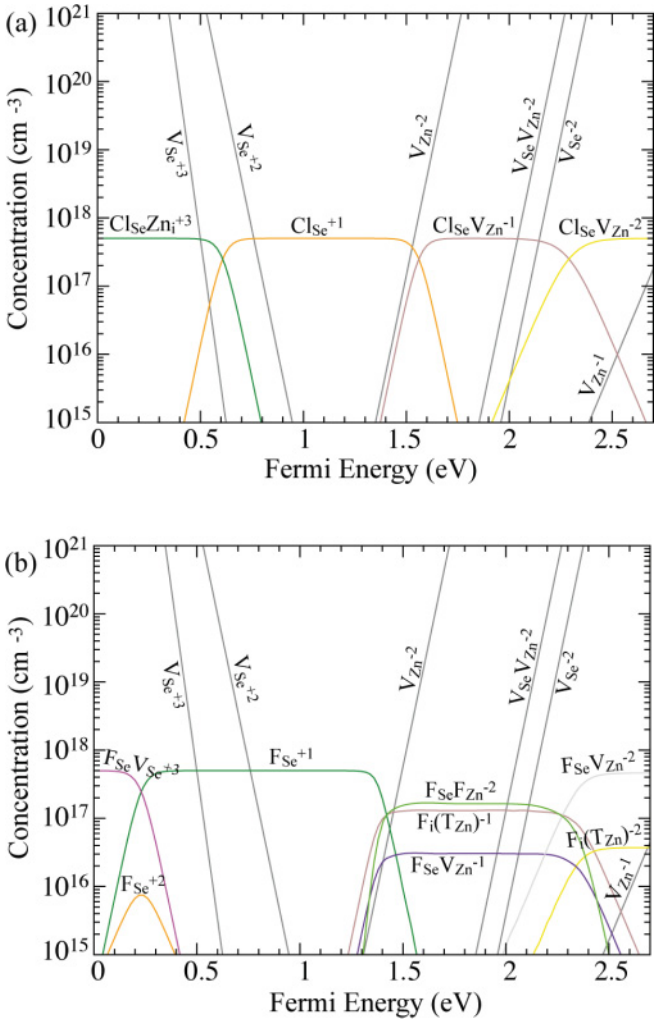

FIG. 3. (Color online) Defect concentrations at $\lambda = 0$ (Zn-rich conditions). The total concentration of Cl or F atoms in each case was kept fixed at $5 \times 10^{17}/cm^3$, and the chemical potential was recalculated at each point to meet this target concentration. (a) Chlorine defects. (b) Fluorine defects.

should have a lower formation energy than Cl_{Se} at low Fermi energies, while Pöykkö *et al.* give a relatively higher formation energy for $Cl_{Se}V_{Se}^{+3}$ and claim that $Cl_{Se}Zn_i$ is only stable in the +1 charge configuration.

Figure 2(b) shows the equivalent results for fluorine, equivalently with $\mu_F = \frac{1}{2}E_{DFT}(F_2)$. The most noteworthy difference here is that some double defects (two F atoms in close proximity) have low formation energies, respectively, $F_{Se}F_{Se}$ and $F_{Se}F_{Zn}$. In the case of chlorine, all double defects have high formation energies, such that they do not appear in Fig. 2(a), being above the top of the scale. This is not the case for fluorine, where $F_{Se}F_{Zn}$ is the most stable defect at high Fermi energies. This could indicate that F defects might tend to group pairwise or even as defect clusters consisting of multiple F atoms, while Cl defects do not show this tendency. In $F_{Se}F_{Zn}$ (−2), the two F atoms relax toward a position close to the Se site. In this position, they bind with approximately 20% shortened bonds to the three surrounding zinc atoms only, while the Zn site is left vacant.

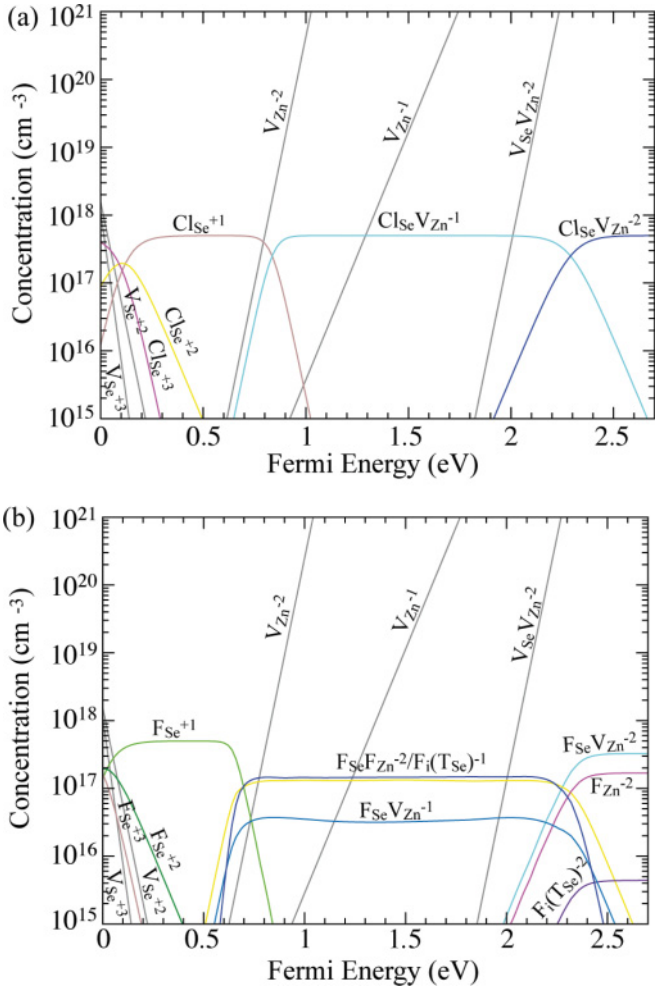

FIG. 4. (Color online) The same as Fig. 3 at $\lambda = 1$ (Se-rich conditions). (a) Chlorine defects. (b) Fluorine defects.

Figure 3 shows the concentration of defects as a function of the Fermi energy. Differently from Fig. 2, for which the data were obtained with a fixed chemical potential, the data of Fig. 3 were obtained by using a fixed impurity concentration equal to $5 \times 10^{17}/\text{cm}^3$ for all situations. This concentration value is introduced in Eq. (9). The chemical potential is calculated for each point in the graph, keeping the impurity concentration fixed. The reason for applying this method, as explained before, is that the impurity concentration can be measured and controlled during crystal growth, while the chemical potential cannot (especially for MBE growth, which is a nonequilibrium process).

Despite the different calculation methods, Figs. 2 and 3 show very similar results. The most stable defects (lowest formation energy in Fig. 2 and highest concentration in Fig. 3) are the same in both cases, with only small discrepancies at the high-Fermi-energy end for fluorine defects.

Figure 4 shows the concentrations for the $\lambda = 1$ condition, that is, Se-rich. V_{Se} and defects containing V_{Se} become more prevalent; V_{Zn} and defects containing V_{Zn} become less prevalent.

The comparison of the formation energies for the most relevant point defects obtained within the GGA and HSE approximations to the electron-electron interaction shown in Table V indicates that the energetical ordering calculated within DFT-GGA is reliable, whereas absolute values for the formation energies should be considered with caution.

V. CONCLUSIONS

In summary, the general picture is quite similar for Cl and F defects. Cl_{Se}^{+1} and F_{Se}^{+1} are the most stable defects in a wide range of Fermi energies, from about 0.6 to 1.4 eV. The +2 charge states of Cl_{Se} and F_{Se} are considerably less stable. At higher Fermi energies, negatively charged complexes consisting of an impurity atom and a zinc vacancy become important. The most important difference between Cl and F is the appearance of double defects ($F_{Se}F_{Zn}$) and interstitials (F_i), which do not appear in the case of chlorine.

Thus, the photoemission centers identified in Ref. 7 are most likely caused by a substitutional fluorine atom (F_{Se}), although a complex with a zinc vacancy or even an interstitial fluorine are possible alternatives, which cannot be excluded by our results.

ACKNOWLEDGMENTS

The authors would like to thank PC^2 in Paderborn and the high-performance computing center (HLRS) in Stuttgart for computational resources, and the DFG (Deutsche Forschungsgemeinschaft) for financial support.

[1] D. B. Laks, C. G. VandeWalle, G. F. Neumark, P. E. Blöchl, and S. T. Pantelides, Phys. Rev. B **45**, 10965 (1992).
[2] A. García and J. E. Northrup, Phys. Rev. Lett. **74**, 1131 (1995).
[3] S. Pöykkö, M. J. Puska, and R. M. Nieminen, Phys. Rev. B **57**, 12164 (1998).
[4] S. Pöykkö, M. J. Puska, and R. M. Nieminen, Phys. Rev. B **57**, 12174 (1998).
[5] K. Saarinen, T. Laine, K. Skog, J. Makinen, P. Hautojarvi, K. Rakennus, P. Uusimaa, A. Salokatve, and M. Pessa, Phys. Rev. Lett. **77**, 3407 (1996).
[6] J. Gebauer, R. Krause-Rehberg, M. Prokesch, and K. Irmscher, Phys. Rev. B **66**, 115206 (2002).
[7] K. Sanaka, A. Pawlis, T. D. Ladd, K. Lischka, and Y. Yamamoto, Phys. Rev. Lett. **103**, 053601 (2009).
[8] G. Kresse and D. Joubert, Phys. Rev. B **59**, 1758 (1999).
[9] J. P. Perdew, J. A. Chevary, S. H. Vosko, K. A. Jackson, M. R. Pederson, D. J. Singh, and C. Fiolhais, Phys. Rev. B **46**, 6671 (1992).
[10] A. V. Krukau, O. A. Vydrov, A. F. Izmaylov, and G. E. Scuseria, J. Chem. Phys. **125**, 224106 (2006).
[11] C. G. V. de Walle and J. Neugebauer, J. Appl. Phys. **95**, 3851 (2004).
[12] K. Reuter, C. Stampfl, and M. Scheffler, in *Handbook of Materials Modeling, Part A Methods*, edited by S. Yip (Springer, Berlin, 2005), pp. 149–234.
[13] W. Chen, C. Tegenkamp, H. Pfnür, and T. Bredow, Phys. Rev. B **82**, 104106 (2010).
[14] L. Hernandez, O. de Melo, M. Melendez-Lira, Z. Rivera-Alvarez, and I. Hernandez-Calderon, J. Vac. Sci. Technol. A **14**, 2269 (1996).